Contaminants in Aquatic and Terrestrial Environments

Characteristics and Sinking Behavior of Typical Microplastics including the Potential Effect of Biofouling: Implications for Remediation

Michiel Van Melkebeke, Colin R. Janssen, and Steven De Meester

Environ. Sci. Technol., **Just Accepted Manuscript** • DOI: 10.1021/acs.est.9b07378 • Publication Date (Web): 18 Jun 2020

Characteristics and Sinking Behavior of Typical Microplastics including the Potential Effect of Biofouling: Implications for Remediation

Michiel Van Melkebeke,[†,‡] Colin Janssen,[†] and Steven De Meester[*,‡]

†*Laboratory of Environmental Toxicology and Aquatic Ecology, Coupure Links 653, B-9000, Ghent, Belgium*

‡*Department of Green Chemistry and Technology, Graaf Karel de Goedelaan 5, 8500, Kortrijk, Belgium*

E-mail: Steven.DeMeester@UGent.be

Abstract

Microplastics are ubiquitous pollutants within the marine environment, predominantly (> 90 %) accumulating in sediments worldwide. Despite the increasing global concern regarding these anthropogenic pollutants, research into the remediation of microplastics is lacking. Here, we examine those characteristics of microplastics that are essential to adequately evaluate potential remediation techniques such as sedimentation and (air) flotation techniques. We analyzed the sinking behavior of typical microplastics originating from real plastic waste samples and identified the best-available drag model to quantitatively describe their sinking behavior. Particle shape is confirmed to be an important parameter strongly affecting the sinking behavior of microplastics. Various common shape descriptors were experimentally evaluated on their ability to appropriately characterize frequently occurring particle shapes of typical microplastics such as spheres, films and fibers. This study is the first in this field to include film particles in its experimental design, which were found to make up a considerable fraction of marine pollution and are shown to significantly affect the evaluation of shape-dependent drag models. Circularity χ and sphericity Φ are found to be appropriate shape descriptors in this context. We also investigated the effect of biofouling on the polarity of marine plastics and estimated its potential contribution to the settling motion of initially floating microplastics based on density-modification. It is found that biofouling alters the polarity of plastics significantly, this is from (near) hydrophobic (i.e. water contact angles from 70 to 100 °) to strong hydrophilic surfaces (i.e. water contact angles from 30 to 40 °) rendering them more difficult to separate from sediment based on polarity as primary separation factor. Thus, next to providing a better understanding of the fate and behavior of typical marine microplastics, these findings serve as a fundamental stepping stone to the development of the first large-scale sediment remediation technique for microplastics to answer the global microplastic accumulation issue.

Introduction

The exponential increase in worldwide plastic production currently translates to an annual production of nearly 400 million metric tons.[1] Combined with a poor waste management system this results in an estimated 4.8 - 12.7 million metric tons of plastic waste entering the oceans every year.[2] Due to physical, chemical and biological processes, such as fragmentation and photodegradation, this plastic debris breaks down into small particles.[3] Microplastics are those plastic particles that are smaller than 5 mm but larger than 1 µm. They are proven to be ubiquitous pollutants within the marine environment and predominantly (94 - 99 %) accumulate on the seafloor.[4–6] Phenomena such as biofouling and marine snow are reported to be large contributors to the latter.[7–9] To date, predictions estimate that the global average concentration of microplastics in intertidal sediments is 32 - 144 particles kg^{-1} and about 1.5 - 6.7 particles kg^{-1} in deep sea sediments.[10] Considering that microplastics have been found in the digestive tract of over 300 different marine species, their environmental impact is of major concern worldwide.[11] Next to severe blockage of feeding appendages, chemical leaching of potentially harmful additives may contribute to the detrimental effects of marine microplastic pollution.[12] In addition, by contaminating the human food chain, considerable microplastic exposure can pose a threat to human food safety. However, at present, the associated risks are only marginally understood.[13]

It was during the last decade that scientific interest led to a large number of publications analyzing the abundance, occurrence, sources and impact of microplastics.[14–16] However, there is hardly any literature related to the remediation of these marine pollutants. Given the growing concern related to the microplastic pollution across the globe, research into the remediation of microplastics is imperative. Considering that seafloor sediment represents the most important sink for marine microplastics, separation techniques that can remove microplastics from sediment mixtures are particularly valuable in this context. Typically, one could consider 3 separation factors for a mixture of microplastics and sediment: size, density and polarity (Table 1). With respect to particle size, there is a significant overlap to be expected between sediment and microplastic particles. As stated before, microplastics are defined between 1 µm and 5 mm. Marine sediment particles vary greatly in size depending on their geographic location, yet they are mostly allocated to either the mud fraction or the sand fraction.[17] The mud fraction involves particles smaller than 63 µm, while the sand fraction consists of particles between 63 µm and 2 mm.[18] This implies that particle size is not a good separation factor in this context. Regarding density, sediment is generally characterized by a density of $2650\,\mathrm{kg\,m^{-3}}$, while the density of the most common plastic types, namely high density polyethylene (HDPE), low density polyethylene (LDPE), polypropylene (PP), polyamide (PA), polyvinyl chloride (PVC), polyethylene terephthalate (PET) and polystyrene (PS),[1,19] rarely exceeds $1400\,\mathrm{kg\,m^{-3}}$. Furthermore, sediment is typically considered as hydrophilic,[20,21] while the polarity of plastics predominantly suggests (near) hydrophobic behavior.[22,23] As a result, sedimentation and (air) flotation techniques appear to be promising remediation techniques since they involve density and/or polarity as their primary separation factor(s).[24]

Table 1: Characterization of sediment and microplastics with respect to 3 typical separation factors: size, density and polarity. The latter is represented by the water contact angle expressed in degrees: water contact angles $< 90\,^{\circ}$ indicate a hydrophilic polarity, water contact angles $> 90\,^{\circ}$ indicate a hydrophobic polarity.

Component	Size range d_p (mm)	Density ρ_p ($\mathrm{kg\,m^{-3}}$)	Water contact angle θ (°)
SEDIMENT			
Mud fraction	< 0.063	2400 – 2700	15 – 60
Sand fraction	0.063 – 2		
MICROPLASTICS			
PP		890 – 920	90 – 117
LDPE		910 – 930	78 – 104
HDPE		930 – 970	78 – 104
PVC		1200 – 1450	80 – 94
PET	0.001 – 5	1300 – 1400	63 – 83
PS		1040 – 1100	73 – 91
PA		1020 – 1150	61 – 96
PC		1150 – 1250	73 – 88
PUR		870 – 1420	67 – 89

However, other factors such as particle shape strongly affect the sinking behavior,[25] which is essentially what determines the performance of the separation process. In addition, biofouling is expected to alter a particle's density as well as its polarity, which in turn affects its sinking behavior and hence potentially changes the separation performance of potential remediation techniques. Considering particle shape, a lot of different geometries have been reported for microplastics such as spheres, granules, films and fibers.[26,27] These typically irregular shapes strongly affect the sinking behavior of particles.[25] Kowalski et al. (2016) were the first to acknowledge that experimental studies are indispensable to gain a better understanding of the sinking behavior of microplastics and the correlated effect of particle shape.[28] The work done by Khatmullina et al. (2017) highlights the effect of particle shape on the sinking behavior of microplastics and argues the need for experiments with real microplastics of different shapes.[29] Recent experimental studies by Waldschläger et al. (2019)

and Kaiser et al. (2019) contribute to the better understanding of the sinking behavior of microplastics by including particles of different shapes.[30,31] However, these studies did not include films, which is a common and particular shape of plastic that is expected to have a large impact on sinking behavior. Packaging represents the most dominant market sector in the plastic industry (i.e. share of ± 40 %),[32] implying a high significance of film particles in microplastic pollution, which is not addressed by current scientific research. Thus, next to adopting real plastic waste samples, film particles are included in this study, which adds an important layer to the experimental design. Regarding biofouling of (micro)plastics, research is also limited. The study by Fazey et al. (2016) provided the first estimates of the longevity of plastic debris at the ocean surface.[33] Kooi et al. (2017) developed the first theoretical model to simulate the effect of biofouling on the fate of microplastics and predicted significant settling movement of initially floating microplastics.[8] Kaiser et al. (2017) experimentally demonstrated that biofouling enhances the deposition of microplastics to marine sediments.[7] However, research regarding the effects of biofouling on the polarity of plastic particles and the associated implications for the technological separation of typical microplastics is lacking.

Therefore, in order to evaluate potential remediation techniques for the removal of microplastics from marine sediments, a profound understanding of the sinking behavior of typical microplastics and an analysis of their relevant physiochemical characteristics are essential. To that end, we investigate the sinking behavior of microplastics originating from real plastic waste samples and analyze the effect of biofouling on the characteristics of different plastic types, in particular on the polarity. To identify the most appropriate drag model to quantitatively describe the sinking behavior of typical microplastics, a comparison is made between different shape-dependent drag models such as those proposed by Haider et al. (1989), Ganser (1993), Dellino et al. (2005), Dioguardi et al. (2018) and Waldschläger et al. (2019) among others.[30,34–37] The drag model that best fits our dataset may be used to evaluate potential remediation techniques and offers valuable insights into the fate of typical marine microplastics. Furthermore, the findings presented in this study may be incorporated in future numerical modelling of the transportation behavior of marine microplastics.[38]

In summary, the main objective of this paper is to provide new fundamental insights into the characteristics and sinking behavior of typical microplastics including the potential effects of biofouling with the aim to support the development of large-scale remediation of marine microplastics. For this purpose, four subobjectives are defined which will be reflected throughout this paper. First, to analyze the sinking behavior of typical microplastic particles, including films in particular. Second, to experimentally determine the best-available drag model for typical microplastics. Third, to examine the (potential) effects of biofouling on the characteristics of microplastics. And fourth, to reflect on the implications of our findings for the remediation of marine microplastics.

Materials and methods

Generation of microplastics from municipal plastic waste. Microplastics were generated from municipal plastic waste gathered at a Flemish waste collection company that serves a population of 281,000 people and processes both domestic and commercial waste. Seven different plastic product types were chosen based on their frequency of occurrence, their main plastic type and their physical structure to account for the wide variety of plastic litter found in the marine environment: beverage bottles composed of PET, cleansing-liquid bottles composed of HDPE, flowerpots composed of PP, food containers composed of PS, beverage shrink wrap composed of PE, food packages composed of PE and pieces of broken construction pipes composed of PVC (Table 2). After cleaning and washing the plastic items with deionized water, each product type was shredded separately. For the two film product types, namely the beverage shrink wrap and the food packages, a Hellweg Granulator (340/150) was used in combination with liquid nitrogen to reduce the film's flexibility. The other product types were milled using a Shini Granulator (16N/20N) with the exception of the broken construction pipes which were manipulated with a traditional miter saw to produce fibers. All generated plastic particles were sieved by using an Endecott Sieve Shaker to target the microplastic size range (from 1 µm to 5 mm). Subsequently, 20 particles were selected per product type, which rendered a total of 140 different microplastic particles.

Table 2: Overview of the plastic (waste) products used in the sinking experiments containing information about the main plastic type and the dominating shape class of the 20 corresponding selected particles per product.

Product	**Plastic type**	**Shape class**
Beverage bottles	PET	Granular
Cleansing-liquid bottles	HDPE	Granular
Flowerpots	PP	Granular
Food Containers	PS	Granular
Beverage shrink wrap	PE	Film
Food packages	PE	Film
Construction pipe pieces	PVC	Fiber

The selected particles were individually characterized by mass with a Mettler Toledo AX105 analytical balance. The density was derived by means of a Precisa Density Kit (350) from the measurements of particles originating from the same products yet of greater mass (i.e. > 0.1 g) due to accuracy limitations. Afterwards, the volume of each particle V_p (m^3) was calculated. The following expression was used to determine the volume-equivalent sphere diameter d_p (m):

$$d_p = \sqrt[3]{\frac{6}{\pi} V_p} \tag{1}$$

Subsequently, the volume-equivalent sphere surface area A_{sph} (m^2) was calculated. To quantify the irregular shape of the particles, a Keyence Digital Microscope (VHX-500FE) was used to generate high resolution 2D-images (SI1 of the Supporting Information). In combination with the image analysis software ImageJ, various common shape descriptors were calculated. The longest, intermediate and shortest principal axis of the best-fit ellipsoid as defined by Kumar et al. (2010)[39] are often an intrinsic part of a particle's shape analysis and are typically used to derive several shape descriptors. These principal axes were obtained by combining the measurements of a Mitutoyo Digimatic Indicator with the data gathered from the 2D-image analysis to attain three-dimensional information. The complete stepwise calculation process for the (shape) characterization of a particular microplastic particle is included in SI2 of the Supporting Information.

Measuring sinking rates of typical microplastics. To measure the terminal sinking velocity u_t ($\mathrm{m\,s^{-1}}$) of the microplastic particles, a traditional cylindrical settling column of 45 cm height and 10 cm in diameter was used. Depending on the density of the particle, deionized water (density $\rho_f = 1000\,\mathrm{kg\,m^{-3}}$) or ethanol (density $\rho_f = 790\,\mathrm{kg\,m^{-3}}$) was used as settling medium. The sinking experiments were performed in a temperature-controlled room to avoid fluctuations in viscosity of the medium between measurements. Prior to the sinking velocity measurements, the microplastic particles were submerged in a beaker filled with the corresponding medium at the same temperature to avoid electrostatic discharge at the surface of the particles.[28] The latter might affect the sinking behavior of plastic particles, which is undesirable during the experiments. After submersion in the beaker, the particles were individually transferred to the top of the settling column and gently released in the fluid by using tweezers. Time recording started 20 cm below the surface of the medium to ensure that the particle reached its terminal velocity. More specifically, the time a particle needed to cross a distance of two times 10 cm was measured by means of an HDR Camera at 100 frames per second. Since the particles were not expected to be smaller than 0.5 mm, the use of backlit-imaging was deemed unnecessary. Given the measured sinking time and the predefined travelled distance, the terminal sinking velocity of each individual particle was calculated.

To validate the measured sinking velocities, two different plastic types of perfectly round references spheres were used. PP spheres (PPS Cospheric) with a certified mean diameter of 2.45 ± 0.05 mm and a density of $900\,\mathrm{kg\,m^{-3}}$ were used in combination with ethanol, while PS spheres (PSS Cospheric) with a certified mean diameter of 1.94 ± 0.05 mm and a density of $1050\,\mathrm{kg\,m^{-3}}$ were used in combination with deionized water as the operating medium. The two average values of 10 successive sinking velocity measurements for both plastic types were compared to theoretical sinking velocities $u_{t,th}$ ($\mathrm{m\,s^{-1}}$) calculated by using the reference law for spheres formulated by Dietrich (1982).[40] This formula was recently verified for spherical microplastics by Kowalski et al. (2016)[28] and represents a modification of the traditional Stokes equation.

The average measured sinking velocity of the reference PS spheres in water was 31 ± 3 mm $\mathrm{s^{-1}}$ and of the reference PP spheres in disolol 68 ± 8 mm $\mathrm{s^{-1}}$. By means of the reference law for spheres derived by Dietrich (1982), theoretical sinking velocities of 29.7 and 63.7 mm $\mathrm{s^{-1}}$, respectively, were calculated. The theoretical values do not deviate more than 1 times the standard deviation of the average measured sinking velocity. Therefore, it is concluded that the applied methodology to measure the sinking velocity is valid and that the results obtained during the sinking experiments are reliable. A figure illustrating the fit of the measured sinking velocities of the certified calibration spheres to the reference law by Dietrich (1982) is provided in SI3 of the Supporting Information.

Evaluation of shape-dependent drag models. Hydrodynamic drag is an important parameter affecting the sinking behavior of particles moving in a liquid.[41] The dimensionless drag coefficient C_D is used to quantify this drag force. For spherical particles, well-defined relationships have been derived linking the drag coefficient with the particle Reynolds number.[34,42] However, for non-spherical particles the drag coefficient depends on both the particle Reynolds number and the particle shape. The dimensionless particle Reynolds number Re_p is a function of fluid properties (i.e. density and viscosity), the particle diameter and the terminal settling velocity of the particle, and provides information about the flow regime. Particle shape is a parameter that is more difficult to quantify. As previously discussed, dimensionless shape descriptors are used for this purpose. To determine which (combination of) shape descriptor(s) describes the effect of particle shape on the sinking behavior of microplastics most accurately, 11 different drag models were compared and evaluated based on our dataset (Table 3). The following 7 shape descriptors are used in these drag models: circularity χ, sphericity Φ, Corey Shape Factor CSF, Powers Index P, particle aspect ratio φ, particle flatness $\mathcal{F}$ and particle elongation e. More information on these shape descriptors can be found in SI2 of the Supporting Information and is available in the corresponding reference (Table 3). Each drag model is empirically derived for a particular range of particle Reynolds numbers (Table 3). In order to experimentally compare and evaluate the different drag models, the average error AE (%) and the root mean squared error RMSE (%) were calculated as measures of fit for the different drag models. The corresponding equations are presented in SI4 of the Supporting Information.

Measuring contact angles of plastic sheets subjected to biofouling. The contact angle θ (°) of a solid surface provides a measure of polarity. It is the angle formed by the intersection of the liquid-solid interface and the liquid-vapor interface when a liquid droplet rests on a solid surface. In case the water contact angle is less than 90°, the solid surface is said to be hydrophilic, while a water contact angle greater than 90° indicates a hydrophobic surface. In other words, low contact angles are observed when the liquid spreads on the surface, while large contact angles are observed when the liquid minimizes its contact with the surface and forms a compact droplet.

To investigate the effect of marine biofouling on the polarity of different plastic types, six of the most common plastic types were selected: HDPE, LDPE, PP, PVC, PET and PS.[1,19] Corresponding pellets were extruded to form long sheets of plastic, which were subsequently cut to produce 10 sheets of 2 by 4 cm for each plastic type. In addition, six different plastic consumer products composed of PP were added to the experiments to examine the effect of additives such as colorants. To induce biofouling, the plastic sheets and consumer products were fixated in a tank filled with seawater. To that end, the sheets were perforated with a soldering iron to allow strapping with thin wires. The plastic sheets with a density greater than the density of seawater were fixated at the top, while the plastic sheets with a lower density were fixated at the bottom of the tank. This was realized by means of water-resistant wires and sand-filled weights. The consumer products composed of PP were analogously perforated and held underwater. An image of the biofouling aquarium setup is

Table 3: Overview of the 11 shape-dependent drag models that were evaluated on their applicability to typical microplastics containing information about the applied parameters (expressed as a function of the used shape descriptors or the particle diameter d_p), the associated experimental particle Reynolds number range and the corresponding reference. Seven different shape descriptors are used: Corey Shape Factor (CSF), Powers Index (P), sphericity (Φ), circularity (χ), aspect ratio (φ), flatness ($\mathcal{F}$) and elongation (e).

Drag model	**Parameters**	**Re$_\mathbf{p}$ range**	**Reference**
$u_t = \sqrt[3]{\frac{(\rho_p - \rho_f)}{\rho_f}\, g\, \nu\, R_3\, 10^{R_1+R_2}}$	$R_1 = \mathrm{f}(d_p)$, $R_1 = \mathrm{f}(d_p$, CSF), $R_2 = \mathrm{f}(d_p)$, $R_3 = \mathrm{f}(d_p$, CSF, P)	$0.07 < Re_p < 5 \times 10^4$	Dietrich (1982)[40]
$C_D = \frac{24}{Re_p}\,(1 + A\, Re_p^B) + \frac{C}{1+\frac{D}{Re_p}}$	$A = \mathrm{f}(\Phi, \Phi^2)$, $B = \mathrm{f}(\Phi)$, $C = \mathrm{f}(\Phi, \Phi^2, \Phi^3)$, $D = \mathrm{f}(\Phi, \Phi^2, \Phi^3)$	$Re_p < 2.6 \times 10^5$	Haider et al. (1989)[34]
$C_D = \left[\frac{48.5}{(1+4.5\,\beta^{0.35})^{0.8}\, Re_p^{0.64}} + \left(\frac{Re_p}{Re_p+100+1000\,\beta}\right)^{0.32} \frac{1}{(\beta^{18}+1.05\,\beta^{0.8})}\right]^{1.25}$	$\beta = \mathrm{CSF}$	$Re_p < 1.5 \times 10^5$	Swamee et al. (1991)[43]
$C_D = K_2\left[\frac{24}{K_1\, K_2\, Re_p}\,(1 + 0.1118\,(K_1\, K_2\, Re_p)^{0.6567}) + \frac{0.4305}{1+\frac{3305}{K_1\, K_2\, Re_p}}\right]$	$K_1 = \mathrm{f}(\Phi)$, $K_2 = \mathrm{f}(\Phi)$	$Re_p < 2.5 \times 10^4$	Ganser (1993)[35]
$C_D = \frac{0.9297}{\Psi^{1.6}\, Re_p^{0.0799}}$	$\Psi = \mathrm{f}(\Phi, \chi)$	$Re_p > 60$	Dellino et al. (2005)[36]
$C_D = \begin{cases} \frac{24}{Re_p}\,\varphi^{-0.828} + 2\sqrt{1-\varphi} & Re_p \leq 10^2 \\ 1 - \frac{1 - C_D(Re_p = 100)}{900}\,(10^3 - Re_p) & 10^2 < Re_p \leq 10^3 \\ 1 & Re_p > 10^3 \end{cases}$	φ	$0.1 < Re_p < 10^4$	Pfeiffer et al. (2005)[44]
$u_t = \frac{\nu}{d_p}\left[\sqrt{\frac{1}{4}\left(\frac{A}{B}\right)^{\frac{2}{m}} + \left(\frac{4}{3}\frac{d_{**}^3}{B}\right)^{\frac{1}{m}}} - \frac{1}{2}\left(\frac{A}{B}\right)^{\frac{1}{m}}\right]^m$	$A = \mathrm{f}(\mathrm{CSF}, \mathrm{P})$, $B = \mathrm{f}(\mathrm{CSF}, \mathrm{P})$, $m = \mathrm{f}(\mathrm{CSF}, \mathrm{P})$, $d_{**} = \mathrm{f}(d_p)$	$Re_p < 10^5$	Camenen (2007)[45]
$C_D = \begin{cases} \frac{C_{D,sphere}}{Re_p^2\, \Psi^{Re_p^{-0.23}}}\left(\frac{Re_p}{1.1883}\right)^{\frac{1}{0.4826}} & Re_p \leq 50 \\ \frac{C_{D,sphere}}{Re_p^2\, \Psi^{Re_p^{0.05}}}\left(\frac{Re_p}{1.1883}\right)^{\frac{1}{0.4826}} & Re_p > 50 \end{cases}$	$\Psi = \mathrm{f}(\Phi, \chi)$	$0.01 < Re_p < 10^4$	Dioguardi et al. (2015)[46]
$C_D = \frac{24\, K_S}{Re_p}\left[1 + 0.125\left(Re_p\,\frac{K_N}{K_S}\right)^{\frac{2}{3}}\right] + \frac{0.46\, K_N}{1+\frac{5330}{Re_p\,\frac{K_N}{K_S}}}$	$K_S = \mathrm{f}(F_S)$, $K_N = \mathrm{f}(F_N)$, $F_S = \mathrm{f}(\mathcal{F}, e)$, $F_N = \mathrm{f}(\mathcal{F}, e)$	$Re_p < 3 \times 10^5$	Bagheri et al. (2016)[47]
$C_D = \frac{24}{Re_p}\left(\frac{1-\Psi}{Re_p} + 1\right)^{0.25} + \frac{24}{Re_p}\,(0.1806\, Re_p^{0.6459})\,\Psi^{-Re_p^{0.08}} + \frac{0.4251}{1+\frac{6880.95}{Re_p}\,\Psi^{5.05}}$	$\Psi = \mathrm{f}(\Phi, \chi)$	$0.03 < Re_p < 10^4$	Dioguardi et al. (2018)[37]
$C_D = \begin{cases} \frac{3}{\mathrm{CSF} \times \sqrt[3]{Re_p}} & \text{non-fibers} \\ \frac{4.7}{\sqrt{Re_p}} + \sqrt{\mathrm{CSF}} & \text{fibers} \end{cases}$	CSF	$0.1 < Re_p < 10^4$	Waldschläger et al. (2019)[30]

included in SI5 of the Supporting Information.

The tank comprises an aquarium of 120 cm length, 50 cm height and 40 cm width. It was filled with seawater originating from the coast of Flanders and supplemented with biomass scraped from breakwaters nearby. In addition, a concentrated algae batch of 1 L was added.

The latter was obtained by capturing algae with a plankton net dragged over surface water of the North Sea by means of a Belgian research vessel. Salinity and temperature were kept constant in a control room at 25 °C. Oxygen supply and circulation of the water were managed by means of an aeration stone. Time-controlled TL-lamps (OSRAM 36W/840) provided the system with sufficient light and simulated the day/night pattern of natural solar radiation. These conditions were managed to reach the point of adequate biofilm formation (i.e. surface coverage of at least 90 %) on the surface of the plastic sheets and consumer products.

Once the biofilm formation appeared to be sufficiently advanced, the plastic sheets were removed from the tank and subsequently dried at room temperature. Afterwards, the sheets were individually mounted on a fixation bench to create a flat, horizontal surface. To measure the contact angle, a Krüss Drop Shape Analyzer 10 Mk2 was used following the sessile drop method where a single drop of distilled water was dosed on the surface of the solid sample. By means of an HD camera, the integrated software was able to automatically fit an ellipsoid to the curvature of the sessile water droplet. From that, the value of the contact angle was calculated. By repeating this process three times for each sample, the average contact angles of both the bio-fouled and the blanco plastic sheets, including the consumer products, were determined. The blanco measurements were taken prior to submersion in the aquarium and after cleaning with distilled water.

Prediction of density-modification caused by biofouling. Considering that approximately 60 % of the total worldwide plastic production is associated with low-density plastics (i.e. buoyant in seawater)[1] and that over 90 % of marine microplastics end up on the seafloor,[5,6] the role of biofouling in the settling behavior of initially floating microplastics has gained scientific interest.[8,33,48] To explore the significance of density-modification caused by biofouling on the sinking behavior of microplastic particles in the marine environment, theoretical calculations were performed to predict the required biofilm thickness T_b on the surface of low-density microplastics to induce settling. To that end, two extreme shapes were considered, namely a perfect sphere and a thin film. For the density ρ_p of the corresponding microplastic particles, a value of $925\,\mathrm{kg\,m^{-3}}$ is assumed, which is derived by calculating the average density of the two most produced and littered low-density plastic types, namely PE and PP.[1,19] Furthermore, a biofilm density ρ_b of $1100 \pm 100\ \mathrm{kg\,m^{-3}}$ is assumed,[49] which is in line with density measurements performed on the bio-fouled plastic sheets described above. The expression derived to describe the average density of the bio-fouled particle ρ_{bp} ($\mathrm{kg\,m^{-3}}$) is given by:

$$\rho_{bp} = \frac{m_p + m_b}{V_p + V_b} \tag{2}$$

where m_p (kg) is the mass of the microplastic particle, m_b (kg) is the mass of the biofilm on the surface of the particle, V_p ($\mathrm{m^3}$) is the volume of the microplastic particle and V_b ($\mathrm{m^3}$) is the volume of the corresponding biofilm. Rearranging the formula and considering that m_b equals the product of V_b and ρ_b yields the following expression for the volume of the biofilm V_b:

$$V_b = \frac{m_p - \rho_{bp}\,V_p}{\rho_{bp} - \rho_b} \tag{3}$$

Assuming that the density of seawater equals $1025\,\mathrm{kg\,m^{-3}}$, the density of the bio-fouled particle ρ_{bp} is stated to be greater than or equal to $1025\,\mathrm{kg\,m^{-3}}$ in order to induce settling in the marine environment as a direct result of biofouling.

For the case of a spherical microplastic particle, the values of V_p and m_p can be calculated for a given particle diameter d_p. Therefore, the minimum required biofilm volume V_b to induce settling can be determined. Afterwards, the thickness of the required biofilm T_b (m) can be derived as follows:

$$2\,T_b = d_{bp} - d_p \tag{4}$$

where d_{bp} (m) is the diameter of the bio-fouled particle. The factor 2 accounts for the fact that this diameter includes two times the thickness of the biofilm layer on the surface area of the sphere. Considering that the diameter of a sphere can be determined by six times the ratio of its volume over its surface area, substitution of d_{bp} in Equation 4 yields:

$$2\,T_b = \frac{V_{bp}}{A_{bp}}\,6 - d_p \tag{5}$$

where A_{bp} (m^2) is the surface area of the bio-fouled particle. The volume of the bio-fouled particle V_{bp} (m^3) is equal to the sum of V_p and V_b. The surface area of a sphere is determined by π times the diameter squared. However, by assuming that $A_{bp} = \pi\, d_p^2$ the surface area of the bio-fouled particle is considered to be independent of the biofilm thickness T_b. Given that the surface area of a sphere increases with the square of its diameter, this assumption would be a significant overestimation of the required biofilm thickness. Moreover, for a given biofilm thickness T_b, the sphere diameter d_p will increase with two times T_b. Therefore, the following expression is derived to approximate T_b:

$$2\,T_b = \frac{(V_p + V_b)}{\pi\,\left(d_p + 2\,T_b\right)^2}\,6 - d_p \tag{6}$$

This equation yields a third-degree polynomial or cubic polynomial in T_b, where the real solution (as opposed to the complex solution) was approximated by using the extended mathematical Solve packages of Matlab R2018b.

For the case of a thin film microplastic particle, a similar approach is proposed starting from Equation 3 which provides an expression for the biofilm volume V_b. For simplification, the film particle is represented as a flattened cube with sides l_p (m) and a fixed thickness h_p (m). Analogously, the corresponding bio-fouled particle is represented as a flattened cube with sides l_{bp} (m) and thickness h_{bp} (m). Given a constant film thickness $h_p = 0.040$ mm, which is an assumption deduced from the physical characterization of the microplastics in our dataset, and a value for l_p, the minimum required biofilm volume V_b can be calculated for $\rho_{bp} \geq 1025\,\mathrm{kg\,m^{-3}}$. Furthermore, the thickness of the required biofilm T_b can be derived as follows:

$$2\,T_b = l_{bp} - l_p \tag{7}$$

where the factor 2 accounts for the fact that the side l_{bp} of the bio-fouled particle includes two times the thickness of the biofilm layer. Considering the volume and surface area of a flattened cube, the volume of the bio-fouled particle V_{bp} equals $l_{bp}^2\, h_{bp}$ and the corresponding surface area A_{bp} equals $2\, l_{bp}^2 + 4\, l_{bp}\, h_{bp}$. As a result, l_{bp} can be expressed as a function of V_{bp} and A_{bp}, namely $l_{bp} = \frac{4\, V_{bp}\, h_{bp}}{A_{bp}\, h_{bp} - 2\, V_{bp}}$. Therefore, Equation 7 becomes:

$$2\, T_b = \frac{4\, V_{bp}\, h_{bp}}{A_{bp}\, h_{bp} - 2\, V_{bp}} - l_p \tag{8}$$

where V_{bp} can be substituted for the sum of V_p and V_b. Furthermore, h_{bp} is determined as $h_p + 2\, T_b$ and l_{bp} as $l_p + 2\, T_b$, analogous to the case of the spherical microplastic particle. Considering the expression for the surface area of a flattened cube described above, the equation for the required biofilm thickness on the surface of a thin film particle to induce settling in seawater is derived:

$$2\, T_b = \frac{4(V_p + V_b)\,(h_p + 2\, T_b)}{\left[2\,(l_p + 2\, T_b)^2 + 4(l_p + 2\, T_b)\,(h_p + 2\, T_b)\right](h_p + 2\, T_b) - 2\,(V_p + V_b)} - l_p \tag{9}$$

This equation yields a fourth degree polynomial or quartic polynomial in T_b, where the physically meaningful solution was also calculated by using the extended mathematical Solve packages of Matlab R2018b.

By varying d_p and l_p for the case of a spherical and a film microplastic particle respectively, two graphs were constructed that express the predicted biofilm thickness required to increase the density of the bio-fouled particle to a value of $1025\,\mathrm{kg\,m^{-3}}$ (i.e. the assumed density of seawater) in function of a measure of particle size, in particular d_p or l_p.

Results and discussion

Sinking behavior of typical microplastics. The volume-equivalent sphere diameter d_p of the microplastics used in the sinking experiments ranged between 0.63 and 3.48 mm (Table 4).

HDPE particles originating from the cleansing-liquid bottles exhibited the largest particle size between 1.57 and 3.48 mm. The PET, PP, PS, PE (i.e. both beverage shrink wrap and food packages) and PVC microplastics had a particle size between 1.00 - 2.80 mm, 1.62 - 2.61 mm, 1.25 - 2.13 mm, 0.63 - 1.98 mm and 0.64 - 1.61 mm, respectively. The terminal sinking velocity u_t of the microplastics ranged from 5 to 105 $\times 10^{-3}$ $\mathrm{m\,s^{-1}}$, both extremes measured in water as medium, similar to the range reported by Kowalski et al. (2016).[28] The terminal sinking velocities of the microplastics were consistently lower than predicted by the reference law for spheres by Dietrich (1982)[40] (Table 4). On average, the theoretically predicted values were 3 to 4 times greater than the measured values. The reason for this discrepancy lies in the fact that typical microplastics, as used in the sinking experiments, are not spherical. This clearly conflicts with the assumptions made in the reference law. Hence, particle shape is an important parameter strongly affecting the sinking behavior of typical microplastics. In particular, the sinking velocities of film and fibrous microplastics (i.e. the PE and PVC microplastics (Table 2), respectively, in this study, represented by the beverage shrink wrap, food packages and construction pipe pieces) are significantly suppressed by their shape considering that they deviate 3 to 7 times from the theoretical predictions for spheres. This indicates that the drag coefficient C_D of film and fibrous microplastics will be higher compared to spherical or granular microplastics for a given particle Reynolds number Re_p.

Therefore, the importance of appropriately accounting for the shape of microplastics in order to quantitatively describe and predict their sinking behavior is confirmed. Given the number of distinct and irregular shapes of typical microplastics, assessing the shape descriptors in order to identify the most fitting ones is fundamental to the subsequent evaluation of shape-dependent drag models. Table 5 summarizes the results of the shape characterization of the considered microplastics by means of the discussed shape descriptors. From these seven different shape descriptors, it is found that circularity χ makes a good distinction between fibrous and non-fibrous microplastics considering that 85 % of the fibrous PVC particles have a circularity > 3 with an average of 6, while 100 % of the non-fibrous particles

Table 4: Summary of the results of the sinking experiments containing information about the mass m (mg), density ρ_p ($\mathrm{kg\,m^{-3}}$), size d_p (mm), measured sinking velocity $u_{t,meas}$ ($\mathrm{mm\,s^{-1}}$) and theoretical sinking velocity $u_{t,th}$ ($\mathrm{mm\,s^{-1}}$) for spheres as proposed by Dietrich (1982)[40] of the considered microplastic particles. Intervals indicate the minimum and maximum observed values, respectively, of the particles associated with a particular plastic product type.

Product[a]	m (mg)	ρ_p ($\mathrm{kg\,m^{-3}}$)	d_p (mm)	$u_{t,meas}$ ($\mathrm{mm\,s^{-1}}$)	$u_{t,th}$ ($\mathrm{mm\,s^{-1}}$)
BB	0.71 – 15.67	1370 ± 1.51	1.00 – 2.80	18.4 – 104.7	56.7 – 152.2
CLB	1.94 – 21.05	952 ± 0.85	1.57 – 3.48	23.6 – 47.8	51.7 – 114.6
FP	2.12 – 8.92	953 ± 1.18	1.62 – 2.61	26.1 – 44.3	53.4 – 88.7
FC	1.09 – 5.30	1054 ± 1.81	1.25 – 2.13	5.1 – 16.4	18.2 – 34.5
BSW	0.21 – 3.76	950 ± 20.18	0.76 – 1.98	7.0 – 19.9	38.5 – 103.0
FPS	0.13 – 1.63	1013 ± 15.70	0.63 – 1.45	4.5 – 9.1	21.3 – 65.8
CPP	0.20 – 3.11	1432 ± 0.63	0.64 – 1.61	8.0 – 24.8	21.9 – 59.9

[a]BB = Beverage bottles; CLB = Cleansing-liquid bottles; FP = Flowerpots; FC = Food Containers; BSW = Beverage shrink wrap; FPS = Food packages; CPP = Construction pipe pieces

have a circularity < 3 with an average of 1.5. Next to circularity, also elongation e and aspect ratio φ are found to be appropriate shape descriptors to characterize the shape of fibrous microplastics since 90 % of the fibrous PVC particles have an elongation < 0.2 and an aspect ratio < 0.1, while 100 % of the non-fibrous particles have an elongation > 0.2 and an aspect ratio > 0.1. To distinguish film particles from non-film particles, it appears that sphericity Φ is a good shape descriptor considering that 90 % of the film PE particles have a sphericity $<$ 0.2 with an average of 0.1, while 96 % of the non-film particles have a sphericity > 0.2 with an average of 0.5. The flatness shape descriptor $\mathcal{F}$ is also found to be suitable to characterize film particles since 98 % of the film PE particles have a flatness < 0.1 with an average of 0.03, while 89 % of the non-film particles have a flatness > 0.1 with an average of 0.3. The Corey Shape Factor CSF is not able to distinguish between film and fibrous microplastics (i.e. no significant difference is found between the correlation of the CSF of film and fibrous microplastics), but successfully differentiates them from the granular microplastics (i.e. the PET, HDPE, PP and PS microplastics in this study (Table 2)) considering that 98 % of the film and fibrous particles have a Corey Shape Factor < 0.05 with an average of 0.04, while

95 % of the granular particles have a Corey Shape Factor > 0.05 with an average of 0.2. The Powers Index P is significantly lower for fibrous particles compared to the non-fibrous particles, but does not display any meaningful characterization to successfully differentiate different shapes (i.e. no significant differences in correlation are found between the Powers Index values of the different shape classes). The latter shape descriptor is particularly prone to error considering that it requires visual comparison with a preset number of images. Interestingly, no shape descriptor seems to be able to adequately characterize and differentiate all included particle shapes. Only sphericity Φ appears to properly distinguish granular, film and fibrous particles from each other to some extent: 75 % of the film PE particles have a sphericity < 0.15, 75 % of the fibrous PVC particles have a sphericity between 0.15 and 0.40, and 70 % of the granular particles have a sphericity > 0.40.

Table 5: Summary of the shape characterization of the considered microplastic particles by means of the dimensionless shape descriptors discussed in this study: Corey Shape Factor (CSF), Powers Index (P), sphericity (Φ), circularity (χ), aspect ratio (φ), flatness ($\mathcal{F}$) and elongation (e). Intervals indicate the minimum and maximum observed values, respectively, of the particles associated with a particular plastic product type.

Product[a]	**CSF**	**P**	Φ	χ	φ	$\mathcal{F}$	**e**
BB	0.071 – 0.832	1.32 – 3.00	0.22 – 0.97	1.130 – 1.890	0.21 – 0.89	0.092 – 0.879	0.336 – 0.961
CLB	0.110 – 0.364	1.26 – 2.28	0.43 – 0.87	1.274 – 1.815	0.18 – 0.54	0.155 – 0.621	0.284 – 0.939
FP	0.120 – 0.271	1.20 – 4.68	0.43 – 0.90	1.227 – 1.852	0.22 – 0.55	0.144 – 0.477	0.311 – 0.897
FC	0.042 – 0.113	1.14 – 2.88	0.23 – 0.47	1.130 – 2.222	0.17 – 0.46	0.052 – 0.179	0.290 – 0.870
BSW	0.012 – 0.048	1.08 – 2.10	0.10 – 0.28	1.250 – 2.146	0.12 – 0.45	0.015 – 0.069	0.233 – 0.872
FPS	0.004 – 0.061	1.08 – 2.82	0.04 – 0.14	1.163 – 2.174	0.14 – 0.41	0.006 – 0.120	0.261 – 0.818
CPP	0.021 – 0.162	0.42 – 1.38	0.16 – 0.58	1.761 – 14.286	0.02 – 0.20	0.075 – 0.733	0.030 – 0.341

[a]BB = Beverage bottles; CLB = Cleansing-liquid bottles; FP = Flowerpots; FC = Food Containers; BSW = Beverage shrink wrap; FPS = Food packages; CPP = Construction pipe pieces

The aim of these shape descriptors is to effectively and conveniently quantify the shape of a particle so that they can be part of an empirical equation to describe and predict the sinking behavior of non-spherical particles, such as typical microplastics, in different fluids. Deriving such shape-dependent empirical equations has been done by many different scientists, each for a particular type or range of particles, but seldom for microplastics. In the next section, we investigate whether these empirical drag models are applicable to typical microplastics and if so, which drag model performs best.

Determination of best-available drag model for microplastics. The particle Reynolds numbers Re_p of the microplastics used during the sinking experiments ranged from 1 to 300, which corresponds to a non-laminar flow regime considering that Re_p does not drop below 1.[25] The latter is important considering that particle shape affects the terminal sinking velocity u_t in a laminar flow regime only marginally.[25] This explains the similar trend of standard drag curves in the laminar region when comparing different shape-dependent drag models. A standard drag curve gives the relationship between the drag coefficient and the particle Reynolds number. Based on the average error AE and the root mean squared error RMSE, the drag model of Dioguardi et al. (2018) is found to best fit the dataset from the 11 different evaluated shape-dependent drag models (Table 6). The average error of 13.20 % indicates that on average the deviation of the theoretical sinking velocity predicted by the drag model equals 13.20 % of the measured sinking velocity. This deviation is comparable to the performance of drag models within their field of application.[37] The RMSE is an absolute measure of fit of the model to the applied dataset that indicates the standard deviation of the unexplained variance. As a result, a low value of the RMSE corresponds to a good fit. The shape factor Ψ used in the drag model of Dioguardi et al. (2018) (Table 3) is defined by the quotient of the shape descriptor sphericity Φ divided by the shape descriptor circularity χ. This is in alignment with our previous findings which indicated that sphericity is a good shape descriptor to characterize film microplastics and partially distinguish between the different geometries of microplastics, and that circularity is a good shape descriptor to characterize fibrous microplastics.

So far, no other studies used different types of real plastic waste samples to investigate the effects of particle properties on the sinking behavior of microplastics. Particularly films are interesting, with a distinct shape and accounting for an important fraction of microplastic pollution in marine sediments.[50–55] It is found that including films in the analysis, significantly impacts the results related to the best-available drag model. To illustrate, the most

Table 6: Overview of the average error (AE) and root mean square error (RMSE) values of 11 different drag models used to compare and evaluate their performance with respect to the microplastic dataset assembled in this study.

Drag model author(s)	AE [%]	RMSE
Dietrich (1982)[a]	19.43	28.46
Haider et al. (1989)	23.30	30.89
Swamee et al. (1991)	17.44	27.08
Ganser (1993)	20.11	25.75
Dellino et al. (2005)	23.88	30.61
Pfeiffer et al. (2005)	48.46	59.78
Camenen (2007)	29.09	33.04
Dioguardi et al. (2015)	32.49	40.20
Bagheri et al. (2016)	21.44	26.22
Dioguardi et al. (2018)	13.20	19.09
Waldschläger et al. (2019)	29.92	38.32

[a]The corresponding drag model was applicable to only 30 % of the data

recent shape-dependent drag model by Waldschläger et al. (2019),[30] which is a function of CSF as single shape descriptor, performs below average as can be seen from Table 6, despite its unique focus on microplastics. This can be explained by recalling that sphericity Φ is a good shape descriptor to distinguish films from non-film particles and that the Corey Shape Factor CSF is inadequate to make a distinction between film and fibrous particles whereas it is able to successfully differentiate them from the other granular particles. In addition, it was concluded that besides sphericity Φ, no shape descriptor is able to adequately characterize all particle shapes. However, when excluding films from the dataset, the model performance of the expressions by Waldschläger et al. (2019) reaches the top three of the evaluated drag models, i.e. from an AE of 29.92 % to 25.95 %, while the performance of the model by Dioguardi et al. (2018)[37] remains relatively stable, i.e. from an AE of 13.20 % to 14.90 %. Furthermore, Waldschläger et al. (2019) propose two different expressions to distinguish between granular (i.e. pellets and fragments) and fibrous particles by means of CSF, which corresponds to our findings regarding that particular shape descriptor.

In general, all the other shape-dependent drag models used for comparison in this study

(Figure 1) perform inferior to the model proposed by Dioguardi et al. (2018).[37] In addition, it can be seen from Figure 1d that the performance of the drag model by Waldschläger et al. (2019),[30] represented by the solid yellow line at the bottom of the graph, significantly drops for film particles to a corresponding AE of 39.80 %. In contrast, the drag model by Bagheri et al. (2016)[47] performs particularly well when applied to film particles exclusively, approaching the best performance of the model by Dioguardi et al. (2018) with an AE of 8.76 % versus 8.50 %. Scatter plots of the measured terminal sinking velocity $u_{t,meas}$ versus the terminal sinking velocity predicted by the drag models $u_{t,calc}$ visually illustrate their performance (SI6 of the Supporting Information). The scatter plot of the drag model proposed by Dioguardi et al. (2018) is given in Figure 2. Note that the trendline is constructed by means of linear regression and is forced through the origin. Therefore, the corresponding equation is of the type $y = ax$. Consequently, the performance of the drag models can be evaluated based on the ability to reproduce the measured terminal sinking velocities, rather than solely from the correlation coefficient R^2. In that regard, the best possible fit is associated with R^2 approximating a value of 1 and a trendline equation given by $y = x$. The drag model proposed by Dioguardi et al. (2018) shows a high correlation coefficient ($\mathrm{R}^2 = 0.96$) with $y = 0.99\,x$, which indicates an excellent model performance for the considered dataset with a slight tendency to underestimate the actual terminal sinking velocities. This tendency is for the most part attributed to the fibrous microplastics included in the dataset. Thus, it appears that the drag model consistently underestimates the terminal sinking velocity of fibrous microplastics, but predicts the terminal sinking velocity of granular and film microplastics very well (Figure 2).

Potential contribution of biofouling to the sinking behavior of floating microplastics. The predicted required thickness of a biofilm T_b on the surface of a floating microplastic particle in order to increase its density to where it matches the density of the surrounding seawater is represented as a function of particle size in Figure 3. In the case of the spherical microplastic particle, the measure of particle size is its diameter d_p, while

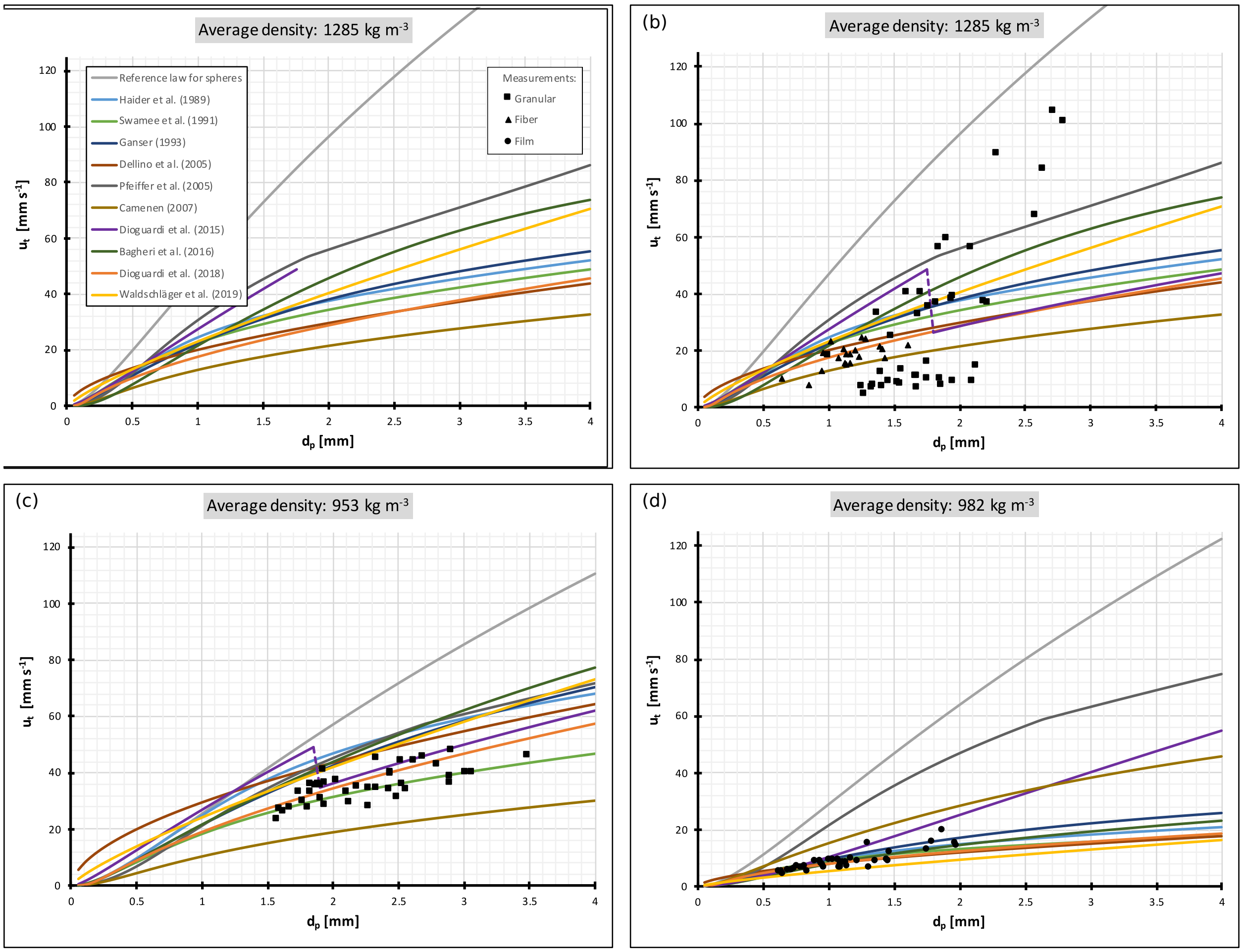

Figure 1: Settling velocity of microplastic particles as a function of particle diameter. The solid grey line represents the reference law for spheres proposed by Dietrich et al. (1982). The colored solid lines represent the shape-dependent drag laws evaluated in this study calculated for the average corresponding shape descriptors as example. Subfigures are included to distinguish between the two different liquid media used during the experiments and additionally isolate film particles from the dataset. (a) Representation of all measurements conducted in this study. (b) Representation of the measurements conducted in water as liquid medium. The corresponding particles show an average density of $1285\,\mathrm{kg\,m^{-3}}$ and the following average values for the shape descriptors: CSF $= 0.152$, P $= 1.515$, $\Phi = 0.374$, $\chi = 0.551$, $\varphi = 0.275$, $\mathcal{F} = 0.239$ and $e = 0.434$. (c) Representation of the measurements conducted in ethanol as liquid medium, excluding film particles. The corresponding particles show an average density of $953\,\mathrm{kg\,m^{-3}}$ and the following average values for the shape descriptors: CSF $= 0.202$, P $= 1.775$, $\Phi = 0.606$, $\chi = 0.672$, $\varphi = 0.336$, $\mathcal{F} = 0.288$ and $e = 0.527$. (d) Representation of the measurements regarding film particles. The corresponding particles show an average density of $982\,\mathrm{kg\,m^{-3}}$ and the following average values for the shape descriptors: CSF $= 0.018$, P $= 1.563$, $\Phi = 0.126$, $\chi = 0.624$, $\varphi = 0.267$, $\mathcal{F} = 0.026$ and $e = 0.522$.

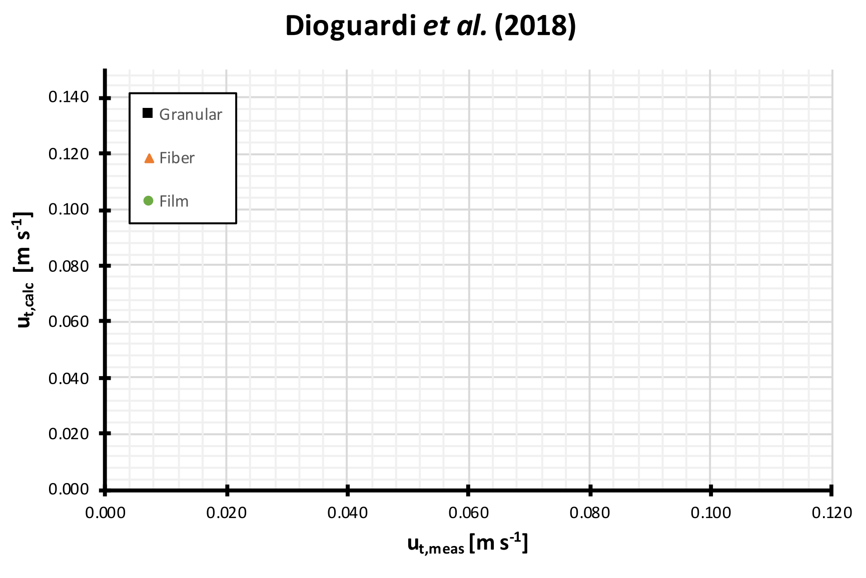

Figure 2: Scatter plot of $u_{t,calc}$ versus $u_{t,meas}$ to evaluate the terminal sinking velocity predicted by the shape-dependent drag model proposed by Dioguardi et al. (2018)[37] applied to the microplastic dataset assembled in this study. The dotted grey line represents the linear regression line of the type $y = ax$ with R^2 the corresponding correlation coefficient. Black squares represent granular particles, green dots film particles and orange triangles fibrous particles as parts of the dataset.

in the case of the film microplastic particle, which is represented by a flattened cube with a fixed thickness h_p of 40 µm, the used measure of particle size is its side l_p. For spherical microplastic particles, the required biofilm thickness is predicted to increase linearly with the particle diameter following $T_b = 0.88\ d_p$ ($R^2 > 0.99$). Consequently, it is expected that a spherical microplastic particle with density $\rho_p = 925\,\mathrm{kg\,m^{-3}}$ and diameter $d_p = 20$ µm requires a biofilm thickness T_b of at least 18 µm to induce settling in seawater as a result of density-modification, while a similar particle with diameter $d_p = 2.0$ mm would require a biofilm thickness T_b of at least 1.8 mm. For film microplastic particles with thickness $h_p = 40$ µm and density $\rho_p = 925\,\mathrm{kg\,m^{-3}}$, the required biofilm thickness T_b increases logarithmically with the particle side l_p. Considering the microplastic size range, it is found that a biofilm thickness $T_b = 35$ µm will induce settling of a film microplastic particle, irrespective of the length of its sides l_p.

Predicting the average thickness of a marine biofilm is challenging considering that it

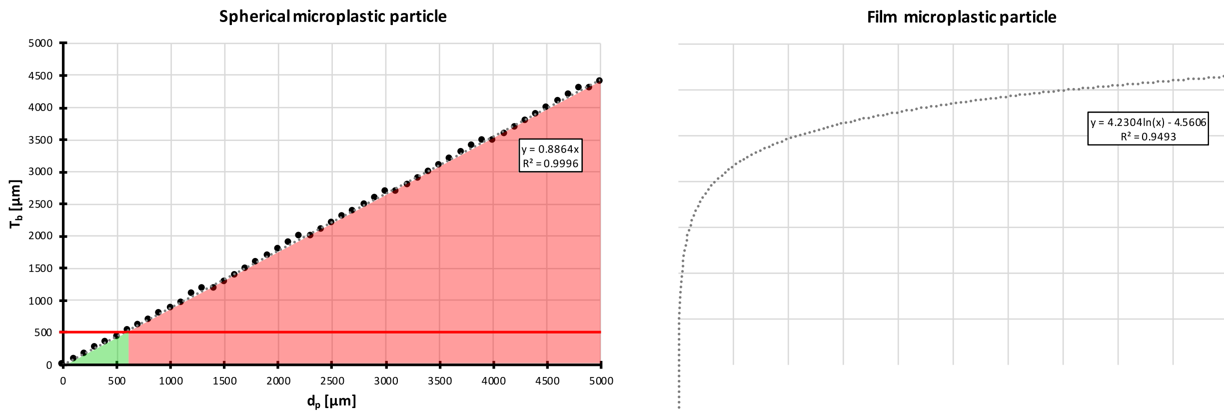

Figure 3: Graphical representation of the predicted biofilm thickness T_b required to increase the density of a microplastic particle with $\rho_p = 925\,\mathrm{kg\,m^{-3}}$ to match the density of seawater (i.e. $1025\,\mathrm{kg\,m^{-3}}$). Two plots are provided with T_b versus d_p (i.e. particle diameter) for a spherical microplastic particle (left) and T_b versus l_p (i.e. flattened cube side) for a thin film microplastic particle with a fixed thickness $h_p = 40$ µm (right). Biofilm thickness values that are assumed to be realistic are highlighted in green, while biofilm thickness values that are assumed to be unlikely to occur in the marine environment are highlighted in red.

depends, among others, on medium composition, substrate nature, present microbial strains and physicochemical properties of the surrounding seawater.[56] For instance, the rate of biofouling is typically higher close to the shore and decreases with increasing depth, while temperature and seasonal changes affect the composition of the corresponding biofilm.[56] In addition, biofilm thickness is generally not homogenous. However, based on existing literature, it is assumed that an average marine biofilm has a thickness ranging from roughly 1 to 500 µm.[56–60] This suggests that spherical microplastics with density $\rho_p = 925\,\mathrm{kg\,m^{-3}}$ and a diameter d_p larger than approximately 600 µm are unlikely to reach an average bio-fouled density of $1025\,\mathrm{kg\,m^{-3}}$ as a direct result of marine biofouling. To illustrate, common plastic resin pellets are typically 1 to 5 mm in diameter. However, it is found that small microplastics (i.e. $<$ 1 mm) represent an important fraction (i.e. 35 to 90 %) of all marine microplastics.[61–65] Furthermore, it appears that biofouling is able to increase the average bio-fouled density of all film microplastic particles with a thickness of 40 µm and a density of $925\,\mathrm{kg\,m^{-3}}$ to where it reaches the density of the surrounding seawater, which is assumed to be $1025\,\mathrm{kg\,m^{-3}}$. In addition, many rigid plastic applications such as trays and bottles generate primarily film-alike microplastics (i.e. the longitudinal axis is significantly greater than the thickness axis). These findings potentially explain why more than 90 % of marine microplastics accumulate on the seabed[5,6] despite the fact that approximately 60 % of the total worldwide plastic production is associated with plastic types having a density smaller than $1025\,\mathrm{kg\,m^{-3}}$.[1] Yet other processes such as the phenomenon of marine snow can also contribute to the sinking behavior of floating microplastics[9] but are less relevant to consider in the case of remediation. Furthermore, biofouling could induce bioflocculation, which in turn may affect the sinking behavior by increasing particle size or altering particle density among other factors.[66] Experiments to confirm this hypothesis could be interesting for future research.

Polarity of marine plastics. Contact angle measurements of the blanco plastic sheets lie within the range of 70 to 100 ° (Table 7), which is in accordance with existing literature.[22,23,67,68] This indicates that the polarity of plastic is situated near the boundary point between hydrophilic (i.e. water contact angle < 90 °) and hydrophobic (i.e. water contact angle > 90 °) behavior. The water contact angles of the six different blanco PP consumer products were very similar yet significantly lower compared to the pure PP sheets, namely on average 81 ° for the consumer products versus 96 ° for the sheets. This suggests that additives such as colorants or surface treatments such as printing inks have a tendency to make the surface of a plastic product more hydrophilic. The bio-fouled plastic surfaces displayed a consistent and significant drop in water contact angle towards values between 30 and 40 ° (Table 7). It also appears that the contact angle of bio-fouled plastic sheets is independent of the plastic type (Table 7). The water contact angles of the bio-fouled PP consumer products were again very similar with an average of 34 °, which lies within the range of the bio-fouled PP plastic sheets. Hence, the addition of additives such as colorants appears to have little effect on the contact angle of bio-fouled plastics. Therefore, it is expected that biofouling will cause microplastics to exhibit an increased hydrophilic behavior and thus more difficult to separate from a sediment mixture.

Table 7: Summary of the water contact angle measurements performed on pure plastic sheets derived from the extrusion of the corresponding pellets, both on blanco plastic sheets and after adequate biofouling. This to examine the effect of marine biofouling on the polarity of plastics.

Plastic type	**Water contact angle θ (°)**	
	Blanco	**Bio-fouled**
LDPE	90.0 ± 2.6	32.3 ± 2.3
HDPE	81.3 ± 2.7	31.8 ± 2.2
PVC	71.5 ± 2.7	31.2 ± 1.8
PET	73.3 ± 1.0	32.4 ± 2.9
PS	83.3 ± 1.1	33.3 ± 2.5
PP	96.1 ± 1.2	35.4 ± 2.7

Implications for remediation of microplastics. Our findings regarding the sinking behavior of typical microplastics contain fundamental information to predict the performance of potential remediation techniques for microplastics. In particular, the identified best-performing drag model may be used to quantitatively estimate the recovery rate of microplastics and compare it to the recovery rate of sediment particles in a sedimentation technique such as centrifugal separation. Typically, particles are assumed to be spherical when evaluating such solid-liquid separation techniques since characterizing particle shape is often time-consuming and/or the impact on the separation performance is assumed to be negligible. However, here we highlight the importance of including a measure of particle shape when evaluating sedimentation techniques for the remediation of microplastics. This because reported particle shapes of microplastics strongly deviate from spheres[26,27] and typical microplastic particle shapes were found to significantly affect the sinking behavior: decreasing the terminal sinking velocity by a factor 3 to 4 on average. By means of comparison, accounting for the significant difference in density between sediment (i.e. $2400\,\mathrm{kg\,m^{-3}}$ – $2700\,\mathrm{kg\,m^{-3}}$) and microplastic particles (i.e. $890\,\mathrm{kg\,m^{-3}}$ – $1450\,\mathrm{kg\,m^{-3}}$) typically decreases the terminal sinking velocity by a factor 2 to 3. Hence, it can be seen that particle shape is not be overlooked when evaluating separation technologies in the context of microplastic remediation as it typically affects the terminal sinking velocity of microplastics even more than the change in density compared to traditional sediment particles. Furthermore, by adopting real plastic waste samples, including films, the identified drag model allows for a more accurate prediction of the microplastic recovery rate of various remediation techniques.

Analysis of marine biofouling on the surface of plastics indicated that bio-fouled microplastics will become more hydrophilic compared to unfouled microplastics. Hence, it is found that biofouling closes the difference in polarity between sediment and microplastic particles. Froth flotation techniques make use of the difference in polarity between solids to separate the most hydrophobic particles from the mixture in a froth layer by selectively adhering air bubbles to the surface of the particles. Consequently, (froth) flotation techniques become less attractive as potential remediation techniques when dealing with bio-fouled microplastics, unless the installation provides a sufficient amount of friction to (partly) detach the corresponding biofilms from the surface of the bio-fouled microplastics. The latter is expected to occur during the pumping stage of the sediment mixture (as part of the remediation process) due to the rather low adhesion of the biofilms to the plastic surfaces experienced during the biofouling experiments. Nevertheless, the degree of biofilm-detachment associated with marine sediments polluted with (micro)plastics requires further research.

In summary, centrifugal separation and (froth) flotation appear to be promising remediation techniques for the removal of microplastics from marine sediments, taking into account the aforementioned complexity with respect to particle shape and biofouling. The effect of particle shape on the remediation process can be evaluated using the drag model of Dioguardi et al. (2018) identified in this study. Biofouling potentially increases the (average) density of microplastics and induces a dominant hydrophilic polarity to the microplastics' surfaces. As a result, biofouling diminishes the difference in density between microplastics and sediment particles, which is particularly unfavorable for centrifugal separation as remediation technique, and closes the difference in polarity between microplastics and sediment particles, which is particularly unfavorable for (froth) flotation as remediation technique. Hence, the development of a large-scale sediment remediation technique for microplastics will prove to be challenging. However, considering the undeniable benefit such a technique can bring to our environment on a global scale, this study seeks to drive research into the remediation of microplastics by sharing scientific reflections dedicated to this matter.

General discussion The main objective of this paper was to provide new fundamental insights into the characteristics and sinking behavior of typical microplastics including the potential effects of biofouling with the aim to support the development of large-scale remediation of marine microplastics. To that end, four subobjectives were aimed at.

First, the sinking behavior of typical microplastics originating from real plastic waste samples was analyzed, including films in particular. This confirmed the importance of particle shape and identified appropriate shape descriptors to quantitatively characterize the most frequently occurring microplastic shapes. We found that the terminal sinking velocity of typical microplastics is on average 3 to 4 times smaller than predicted by the reference law for spheres, and up to 7 times smaller for fibrous microplastics particularly. Circularity is found to be an appropriate shape descriptor to distinguish fibrous microplastics from non-fibrous microplastics and sphericity is found to be an appropriate shape descriptor to distinguish film microplastics from non-film microplastics. In general, sphericity (as defined in this study) appears to be a recommended shape descriptor to include in the shape characterization of typical microplastics.

Second, the best-available, shape-dependent drag model for typical microplastics was experimentally identified, providing fundamental information for the exploration of potential remediation techniques. The drag model of Dioguardi et al. (2018)[37] is concluded to be the most accurate with respect to typical microplastics and can therefore be used to theoretically predict and evaluate the separation performance of potential remediation techniques.

Third, the effects of biofouling on the characteristics of microplastics were examined indicating the potential impact of biofouling on the remediation and fate of microplastics. Biofouling is found to render plastic surfaces more hydrophilic, this is from a water contact angle between 70 and 100 ° to a water contact angle between 30 and 40 °, making them more difficult to separate from sediment mixtures based on polarity. Marine biofouling is also found to be a potential contributor to the settling motion of low-density microplastics (i.e. intrinsically floating in seawater), in particular of film microplastics.

And fourth, a reflection was presented on the direct implications of our findings for the remediation of marine microplastics, demonstrating the opportunities to technologically answer the global microplastic accumulation issue, yet highlighting the associated difficulties. Hence, this study serves as an important step in the development of large-scale remediation techniques for the removal of microplastics from marine sediments.

Acknowledgement

The authors thank Ruben Demets, Pieter Knockaert, Nicolas Mys and Martijn Roosen from Campus Kortrijk for their invested time and efforts during the experiments. Also Nancy De Saeyer from Campus Coupure actively contributed to the successful realization of the experimental phases of this study.

Supporting Information Available

The following files are available free of charge via the Internet at http://pubs.acs.org.

- Supporting_Information.pdf: post-processed 2D-images of all microplastics in the dataset captured by means of a digital microscope (SI1); stepwise calculation example for the (shape) characterization of the microplastics (SI2); experimental validation figure illustrating the fit of the measured sinking velocities of the certified calibration spheres to the selected reference law for spheres (SI3); presentation of applied equations to validate the different drag models (SI4); informative image of the experimental biofouling setup (SI5); scatter plots of the 10 shape-dependent drag models used in this study to evaluate their performance applied to the microplastics dataset (SI6)

- Microplastics_Dataset_VanMelkebeke_et_al_2020.xlsx: the constructed dataset of typical microplastics containing information about their mass, density, volume and shape descriptors added with the model performance evaluation of the 11 drag models discussed in this study, including the corresponding standard drag curves

References

(1) Geyer, R.; Jambeck, J. R.; Law, K. L. Production, uses, and fate of all plastics ever made. *Science Advances* **2017**, *3*, 5.

(2) Jambeck, J. R.; Geyer, R.; Wilcox, C.; Siegler, T. R.; Perryman, M.; Andrady, A.; Narayan, R.; Law, K. L. Plastic waste inputs from land into the ocean. *Science* **2015**,

(3) Browne, M.; Galloway, T.; Thompson, R. Microplastic – an emerging contaminant of potential concern? *Integrated Environmental Assessment and Management* **2007**, *3*.

(4) Cauwenberghe, L. V.; Vanreusel, A.; Mees, J.; Janssen, C. R. Microplastic pollution in deep-sea sediments. *Environmental Pollution* **2013**, *182*, 495–499.

(5) Sherrington, C. *Plastics in the Marine Environment*; 2016; Vol. 6; pp 1–13.

(6) Koelmans, A. A.; Kooi, M.; Law, K. L.; van Sebille, E. All is not lost: deriving a top-down mass budget of plastic at sea. *Environmental Research Letters* **2017**, *12*, 114028.

(7) Kaiser, D.; Kowalski, N.; Waniek, J. J. Effects of biofouling on the sinking behavior of microplastics. *Environmental Research Letters* **2017**, *12*, 124003.

(8) Kooi, M.; Van Nes, E. H.; Scheffer, M.; Koelmans, A. A. Ups and Downs in the Ocean: Effects of Biofouling on Vertical Transport of Microplastics. *Environmental Science and Technology* **2017**, *51*, 7963–7971.

(9) Porter, A.; Lyons, B. P.; Galloway, T. S.; Lewis, C. Role of Marine Snows in Microplastic Fate and Bioavailability. *Environmental Science and Technology* **2018**, *52*, 7111–7119.

(10) Everaert, G.; Van Cauwenberghe, L.; De Rijcke, M.; Koelmans, A. A.; Mees, J.; Vandegehuchte, M.; Janssen, C. R. Risk assessment of microplastics in the ocean: Modelling approach and first conclusions. *Environmental Pollution* **2018**, *242*, 1930–1938.

(11) Kühn, S.; Bravo Rebolledo, E. L.; van Franeker, J. A. In *Marine Anthropogenic Litter*; Bergmann, M., Gutow, L., Klages, M., Eds.; Springer International, 2015; pp 75–116.

(12) Wright, S. L.; Thompson, R. C.; Galloway, T. S. The physical impacts of microplastics on marine organisms: A review. *Environmental Pollution* **2013**, *178*, 483–492.

(13) Barboza, L. G. A.; Vethaak, D. A.; Lavorante, B. R.; Lundebye, A.-K.; Guilhermino, L. Marine microplastic debris: An emerging issue for food security, food safety and human health. *Marine Pollution Bulletin* **2018**, *133*, 336 – 348.

(14) Sundt, P.; Schultze, P.-E.; Syversen, F. *Sources of microplastic-pollution to the marine environment*; 2014; p 86.

(15) Barboza, L.; Gimenez, B. Microplastics in the marine environment: Current trends and future perspectives. *Marine Pollution Bulletin* **2015**, *97*, 5–12.

(16) Kramm, J.; Völker, C. In *Freshwater Microplastics : Emerging Environmental Contaminants?*; Wagner, M., Lambert, S., Eds.; Springer International Publishing: Cham, 2018; pp 223–237.

(17) National Geophysical Data Center, The NGDC Seafloor Sediment Grain Size Database. 1976.

(18) Blott, S.; Pye, K. Particle size scales and classification of sediment types based on particle size distributions: Review and recommended procedures. *Sedimentology* **2012**, *59*, 2071–2096.

(19) Andrady, A. Microplastics in the marine environment. *Marine Pollution Bulletin* **2011**, *62*.

(20) Giese, R. F.; Van Oss, C. J. *Reaction Kinetics and Catalysis Letters*, first edit ed.; CRC Press: Oxford, 2002; Vol. 77; pp 393–394.

(21) Borysenko, A.; Clennell, B.; Sedev, R.; Burgar, I.; Ralston, J.; Raven, M.; Dewhurst, D.; Liu, K. Experimental investigations of the wettability of clays and shales. *Journal of Geophysical Research: Solid Earth* **2009**, *114*, 1–11.

(22) Angu, E.; Drelich, J.; Laskowski, J.; Mittal, K. *Apparent and Microscopic Contact Angles*; CRC Press: Utrecht, The Netherlands, 2000; p 293.

(23) van Oss, C. J. *Interfacial Forces in Aqueous Media*, second edi ed.; CRC Press, 2006; p 456.

(24) Perry, R. H.; Green, D. W. *Perry's Chemical Engineers' Handbook*; Mcgraw-Hill Education - Europe, 1997; p 2641.

(25) Rhodes, M. *Introduction to Particle Technology*, second edi ed.; Wiley: Monash University, Australia, 2008; p 450.

(26) Free, C. M.; Jensen, O. P.; Mason, S. A.; Eriksen, M.; Williamson, N. J.; Boldgiv, B. High-levels of microplastic pollution in a large, remote, mountain lake. *Marine Pollution Bulletin* **2014**, *85*, 156–163.

(27) Karami, A. Gaps in aquatic toxicological studies of microplastics. *Chemosphere* **2017**, *184*, 841–848.

(28) Kowalski, N.; Reichardt, A. M.; Waniek, J. J. Sinking rates of microplastics and potential implications of their alteration by physical , biological , and chemical factors. *MPB* **2016**, *109*, 310–319.

(29) Khatmullina, L.; Isachenko, I. Settling velocity of microplastic particles of regular shapes. *Marine Pollution Bulletin* **2017**, *114*, 871 – 880.

(30) Waldschläger, K.; Schüttrumpf, H. Effects of Particle Properties on the Settling and Rise Velocities of Microplastics in Freshwater under Laboratory Conditions. *Environmental Science & Technology* **2019**, *53*.

(31) Kaiser, D.; Estelmann, A.; Kowalski, N.; Glockzin, M.; Waniek, J. J. Sinking velocity of sub-millimeter microplastic. *Marine Pollution Bulletin* **2019**, *139*, 214 – 220.

(32) PlasticsEurope, *Plastics – the Facts 2017: An analysis of European plastics production, demand and waste data*; 2018; p 16.

(33) Fazey, F. M. C.; Ryan, P. G. Biofouling on buoyant marine plastics: An experimental study into the effect of size on surface longevity. *Environmental Pollution* **2016**, *210*, 354–360.

(34) Haider, A.; Levenspiel, O. Drag Coefficient and Terminal Velocity of Spherical and Nonspherical Particles. *Powder Technology* **1989**, *58*, 63–70.

(35) Ganser, G. H. A rational approach to drag prediction nonspherical particles. *Powder Technology* **1993**, *77*, 143–152.

(36) Dellino, P.; Mele, D.; Bonasia, R.; Braia, G.; Volpe, L. L.; Sulpizio, R. The analysis of the influence of pumice shape on its terminal velocity. *Geophysical Research Letters* **2005**, *32*, 2–5.

(37) Dioguardi, F.; Survey, B. G.; Mele, D.; Dellino, P. A New One-Equation Model of Fluid Drag for Irregularly Shaped Particles Valid Over a Wide Range of Reynolds Number: Aerodynamic drag of irregular particles (corrected). *Journal of Geophysical Research: Solid Earth* **2018**, *123*, 144–156.

(38) Jalón-Rojas, I.; Wang, X.; Fredj, E. A 3D numerical model to Track Marine Plastic Debris (TrackMPD): Sensitivity of microplastic trajectories and fates to particle dynamical properties and physical processes. *Marine Pollution Bulletin* **2019**, *141*, 256–272.

(39) Kumar, R. G.; Strom, K. B.; Keyvani, A. Floc properties and settling velocity of San Jacinto estuary mud under variable shear and salinity conditions. *Continental Shelf Research* **2010**, *30*, 2067–2081.

(40) Dietrich, W. E. Settling Velocity of Natural Particles. *Water Resources Research* **1982**, *18*, 1615–1626.

(41) Crowe, C. T. *Multiphase Flow Handbook*; CRC Press: Boca Raton, New York, 2005; p 1156.

(42) Clift, R.; Gauvin, W. H. Motion of entrained particles in gas streams. *The Canadian Journal of Chemical Engineering* **1971**, *49*, 439–448.

(43) Swamee, P.; Ojha, C. Drag coefficient and fall velocity of nonspherical particles. *Journal of Hydraulic Engineering* **1991**, *117*, 660–667.

(44) Pfeiffer, T.; Costa, A.; Macedonio, G. A model for the numerical simulation of tephra fall deposits. *Journal of Volcanology and Geothermal Research* **2005**, *140*, 273–294.

(45) Camenen, B. Simple and General Formula for the Settling Velocity of Particles. *Journal of Hydraulic Engineering* **2007**, *133*, 229–233.

(46) Dioguardi, F.; Mele, D. A new shape dependent drag correlation formula for non-spherical rough particles. Experiments and results. *Powder Technology* **2015**, *277*.

(47) Bagheri, G.; Bonadonna, C. On the drag of freely falling non-spherical particles. *Powder Technology* **2016**, *301*, 526–544.

(48) Ye, S.; Andrady, A. L. Fouling of floating plastic debris under Biscayne Bay exposure conditions. *Marine Pollution Bulletin* **1991**, *22*, 608–613.

(49) Ro, K. S.; Neethling, J. B. Biofilm Density for Biological Fluidized Beds. *Research Journal of the Water Pollution Control Federation* **1991**, *63*, 815–818.

(50) Claessens, M.; De Meester, S.; Landuyt, L. V.; Clerck, K. D.; Janssen, C. R. Occurrence and distribution of microplastics in marine sediments along the Belgian coast. *Marine Pollution Bulletin* **2011**, *62*, 2199–2204.

(51) Nor, N. H. M.; Obbard, J. P. Microplastics in Singapore's coastal mangrove ecosystems. *Marine Pollution Bulletin* **2014**, *79*, 278 – 283.

(52) Zobkov, M.; Esiukova, E. Microplastics in Baltic bottom sediments: Quantification procedures and first results. *Marine Pollution Bulletin* **2016**, *114*.

(53) Mistri, M.; Infantini, V.; Scoponi, M.; Granata, T.; Moruzzi, L.; Massara, F.; De Donati, M.; Munari, C. Small plastic debris in sediments from the Central Adriatic Sea: Types, occurrence and distribution. *Marine Pollution Bulletin* **2017**, *124*, 435 – 440.

(54) Vaughan, R.; Turner, S. D.; Rose, N. L. Microplastics in the sediments of a UK urban lake. *Environmental Pollution* **2017**, *229*, 10 – 18.

(55) Abidli, S.; Antunes, J. C.; Ferreira, J. L.; Lahbib, Y.; Sobral, P.; Trigui El Menif, N. Microplastics in sediments from the littoral zone of the north Tunisian coast (Mediterranean Sea). *Estuarine, Coastal and Shelf Science* **2018**, *205*, 1 – 9.

(56) Lehaitre, M.; Delauney, L.; Compere, C. *Biofouling and underwater measurements*; 2008; pp 463–493.

(57) Salta, M.; Wharton, J.; Blache, Y.; Stokes, K. R.; Briand, J.-f. Marine Biofilms on artificial surfaces : Structure and dynamics Minireview Marine biofilms on artificial surfaces : structure and dynamics. *Environmental Microbiology* **2013**, *15*, 2879–2893.

(58) Doghri, I.; Rodrigues, S.; Bazire, A.; Dufour, A.; Akbar, D.; Sopena, V.; Sablé, S.; Lanneluc, I. Marine bacteria from the French Atlantic coast displaying high forming-

biofilm abilities and different biofilm 3D architectures. *BMC Microbiology* **2015**, *15*, 1–10.

(59) Li, C.; Zhang, Y.; Yehuda, C. RSC Advances Individual based modeling of Pseudomonas aeruginosa bio fi lm with three detachment. *RSC Advances* **2015**, 79001–79010.

(60) Inaba, T.; Hori, T.; Aizawa, H.; Ogata, A.; Habe, H. Architecture , component , and microbiome of bio fi lm involved in the fouling of membrane bioreactors. *npj Biofilms and Microbiomes* **2017**, *3*.

(61) McDermid, K. J.; McMullen, T. L. Quantitative analysis of small-plastic debris on beaches in the Hawaiian archipelago. *Marine Pollution Bulletin* **2004**, *48*, 790–794.

(62) Browne, M. A.; Galloway, T. S.; Thompson, R. C. Spatial Patterns of Plastic Debris along Estuarine Shorelines. *Environmental Science & Technology* **2010**, *44*, 3404–3409.

(63) Eriksen, M.; Mason, S.; Wilson, S.; Box, C.; Zellers, A.; Edwards, W.; Farley, H.; Amato, S. Microplastic pollution in the surface waters of the Laurentian Great Lakes. *Marine Pollution Bulletin* **2013**, *77*, 177–182.

(64) Song, Y. K.; Hong, S. H.; Jang, M.; Kang, J. H.; Kwon, O. Y.; Han, G. M.; Shim, W. J. Large accumulation of micro-sized synthetic polymer particles in the sea surface microlayer. *Environmental Science Technology* **2014**, *48*, 9014–9021.

(65) Zhao, S.; Zhu, L.; Wang, T.; Li, D. Suspended microplastics in the surface water of the Yangtze Estuary System, China: First observations on occurrence, distribution. *Marine Pollution Bulletin* **2014**, *86*, 562–568.

(66) Shang, Q.; Fang, H.; Zhao, H.; He, G.; Cui, Z. Biofilm effects on size gradation, drag coefficient and settling velocity of sediment particles. *International Journal of Sediment Research* **2014**, *29*, 471–480.

(67) Mittal, K. *Adhesion Aspects of Thin Films*; VSP: Zeist, The Netherlands, 2001.

(68) Mittal, K. *Contact Angle, Wettability and Adhesion*, edition 3 ed.; VSP: Utrecht, 2003; p 293.

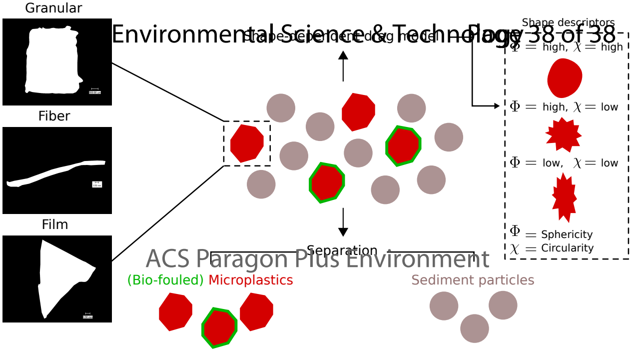
Granular
Fiber
Film
Shape-dependent drag model
Shape descriptors
Φ = high, χ = high
Φ = high, χ = low
Φ = low, χ = low
Φ = Sphericity
χ = Circularity
Separation
(Bio-fouled) Microplastics
Sediment particles